

bradscholars

Analytical model for the suspended sediment concentration in the ice-covered alluvial channels

Item Type	Article
Authors	Wang, F.;Huai, W.;Guo, Yakun
Citation	Wang F, Huai W and Guo Y (2021) Analytical model for the suspended sediment concentration in the ice-covered alluvial channels. Journal of Hydrology. 597: 126338.
DOI	https://doi.org/10.1016/j.jhydrol.2021.126338
Publisher	Elsevier
Rights	© 2021 Elsevier. Reproduced in accordance with the publisher's self-archiving policy. This manuscript version is made available under the CC-BY-NC-ND license (https://creativecommons.org/licenses/by-nc-nd/4.0/)
Download date	2026-04-13 17:44:38
Link to Item	https://bradscholars.brad.ac.uk/handle/10454/18453.2

Analytical model for the suspended sediment concentration in the ice-covered alluvial channels

Feifei Wang^a, Wenxin Huai^{a,*}, Yakun Guo^b

^a *State Key Laboratory of Water Resources and Hydropower Engineering Science, Wuhan University, Wuhan 430072, China*

^b *Faculty of Engineering & Informatics, University of Bradford, BD7 1DP, UK*

E-mail Addresses:

Feifei Wang, ffwang1991@whu.edu.cn;

Wenxin Huai, *Corresponding author, wxhuai@whu.edu.cn;

Yakun Guo, y.guo16@bradford.ac.uk.

Abstract

Ice cover formed on an alluvial channel can significantly alter the flow characteristics, such as the vertical distributions of streamwise velocity and shear stress, and hence the water and sediment transport process. The vertical profile of the suspended sediment concentration in the ice-covered alluvial channels with steady uniform flows is investigated in this study. To calculate the suspended sediment concentration, we are based on the Schmidt O'Brien equation and deduce an analytical model that employs an existing eddy viscosity model and a modified formula of the sediment fall velocity considering the common effects of the upper and lower boundaries. The proposed analytical model is then validated by using available experimental data reported in the literature. The predicted accuracy of the proposed model is evaluated through error statistics by comparing to previous modeled results. The relative concentration profiles of the suspended sediment are subsequently simulated by applying the

23 validated analytical model with different characteristic parameters. Results show that the
24 relative concentration decreases with the increase of both the ice cover roughness and the
25 sediment fall velocity. The uniformity of the relative concentration distribution is closely
26 related to the value of the proportionality parameter σ , revealing the physical mechanism that
27 the more prominent the turbulent diffusion effect is, the more uniform the relative
28 concentration profile is.

29 **Keywords:** Suspended sediment concentration; Ice-covered channel; Analytical model;
30 Modified sediment fall velocity

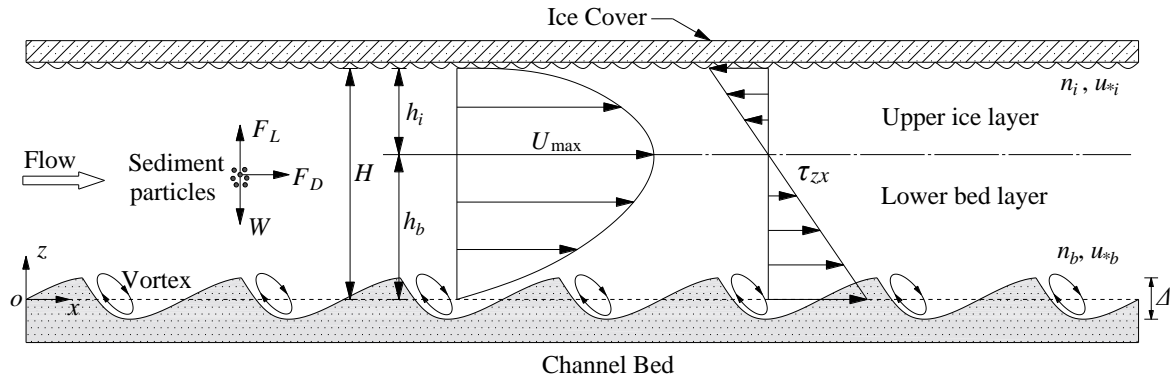
31 **1. Introduction**

32 The flow structure in alluvial channels changes and develops continuously, caused by the
33 interaction between the water flow and the rough river bed (Lane et al., 1996; Sharma et al.,
34 2019; Tayfur and Singh, 2012). In effect, sediment transport, which is mainly controlled by
35 the turbulent flow structure, is the agent of the aforementioned interacted process (Cordier et
36 al., 2019). When the lift force exerted on the sediment particle due to the turbulent diffusion
37 effect is greater than the submerged weight of the sediment particle, the sediment particle will
38 be raised from the channel bed and move forward along with the water flow, thereby forming
39 sediment-laden flow (Brayshaw et al., 1983; Cheng et al., 2020). On the other hand, if the
40 turbulent diffusion effect is weaker than the submerged weight effect of the sediment particle,
41 the suspended sediment particle will be brought back to the channel bed, resulting in the
42 sediment deposition. In engineering practice, the sediment problem is one of the issues that
43 engineers must consider in the construction of all water conservancy projects, such as the
44 selection of a port site, the scheme formulation of the channel dredging and improvement,

45 and the layout of the irrigation and drainage facilities (Peng et al., 2020; Stone and
46 Krishnappan, 2002; Torres et al., 2009; Xia et al., 2016; Yang et al., 2007). Therefore, in
47 light of the non-negligible impact of the sediment movement on the industrial and
48 agricultural production along the channel banks, there is a growing interest in the
49 concentration distribution of the suspended sediment in the alluvial channels.

50 When alluvial channels located in cold regions expose to freezing temperatures, an ice
51 cover will form over the water surface of alluvial channels, significantly altering the flow
52 characteristics and consequently influencing the sediment transport (Chassiot et al., 2020;
53 Ettema, 2002; Lawler, 1993; Turcotte et al., 2011). As shown in the schematic diagram of
54 Fig.1, the ice-covered alluvial channel flow is asymmetric concerning the plane of the zero
55 shear stress due to the different roughnesses and shear stresses on the upper and lower
56 boundaries (Guo et al., 2017; Tsai and Ettema, 1994). The wetted perimeter of the shallow
57 channel is approximately doubled. Both the flow depth and the total boundary shear stress
58 increase and the averaged streamwise velocity decreases (Hoque, 2009; Smith and Ettema,
59 1997; Wang et al., 2020). Given that the total boundary shear stress is certainly distributed
60 between the upper and lower boundaries, the boundary shear stress corresponding to the
61 channel bed (i.e., the lower boundary) is expected to be reduced (Sayre and Song, 1979). The
62 reduction of the bed boundary shear stress and the averaged streamwise velocity can in turn
63 reduce the bedload transport as well as the suspended sediment concentration (SSC), thereby
64 affecting the sediment transport process and hence the river bed morphology. Because
65 knowledge of the SSC profile is related to many engineering and environmental problems,
66 such as the operation and maintenance of a reservoir and the performance of the

67 channel-control structures (Beltaos and Burrell, 2016; Caissie et al., 2014; Ettema et al., 2000;
 68 Gebre et al., 2014), it is necessary to investigate the SSC in the ice-covered alluvial channel
 69 flows.



70

71 **Fig. 1.** Schematic diagram showing the variables affecting water flow and sediment transport in an
 72 ice-covered alluvial channel. The definitions of the physical variables in the figure are presented in the
 73 Nomenclature.

74 Extensive studies have been conducted to investigate the SSC profiles in the fully
 75 developed, two-dimensional (2D) free-surface alluvial channel flows (Cellino and Lemmin,
 76 2004; Jha and Bombardelli, 2011; Kabir and Ahmari, 2020; Miyata et al., 2020; Pal and
 77 Ghoshal, 2017; Rouse, 1937; Umeyama, 1992). However, to the authors' best knowledge,
 78 studies on the SSC profile in the ice-covered alluvial channel flows have been very limited,
 79 except that several studies were carried out to explore the sediment transport using the flume
 80 experiments with narrow flow conditions. Muste et al. (2000) carried out laboratory flume
 81 experiments in an ice-covered sand-bed channel and found that the sediment transport rates
 82 were reduced comparing with that without the ice cover channel flows. Sayre and Song (1979)
 83 performed flume experiments to investigate the effect of a floating ice cover on the sediment
 84 transport features. They divided the flow of the ice-covered channel into two layers, namely

85 the upper ice layer and the lower bed layer, with the maximum streamwise velocity and the
86 zero turbulent shear stress at the interface. Subsequently, the analytical expressions for the
87 vertical turbulent mass transfer coefficient and the SSC were derived by adopting the
88 two-layer approach. Based on the formula of the SSC proposed by Sayre and Song (1979),
89 Knack and Shen (2015) estimated the suspended sediment load and the bed load for the
90 ice-covered channels. Differently, Krishnappan (1983) applied the $k-\varepsilon$ turbulent model to
91 predict the momentum diffusivity distributions in the ice-covered streams and then
92 formulated the concentration distribution curves for the suspended sediment. Similar to the
93 method used by Krishnappan (1983), Lau and Krishnappan (1985) simulated both the SSC
94 profile and the streamwise velocity distribution and then compared the simulated results with
95 their laboratory measurements conducted under different ice-covered conditions. Huang
96 (2014) and Knack (2011) developed a two-dimensional numerical model that coupled the
97 hydro-thermo-ice-sediment dynamics to investigate the effect of the ice cover on the
98 suspended sediment transport in curved channels.

99 The above literature review shows that the previous models predicting the SSC profile for
100 the ice-covered channel flows can be classified as the analytical model and the numerical
101 model, as shown in Table 1. Although the analytical model proposed by Sayre and Song
102 (1979) has a good predictive ability, one needs to know the streamwise velocity profile prior
103 to determining the position of the maximum streamwise velocity for the application of the
104 two-layer hypothesis. The model of the turbulent mass transfer coefficient that is the key
105 factor to obtain the above analytical model consists of three components and is not integrated
106 into a single equation. Furthermore, the turbulent mass transfer coefficient is not deduced

107 rigorously, because Sayre and Song (1979) simply assumed that the turbulent mass transfer
 108 coefficient followed the linear distribution in the central region. The numerical model
 109 presented by Krishnappan (1983) and Lau and Krishnappan (1985) applied the $k-\varepsilon$ turbulent
 110 model. When one applies the numerical model to simulate the SSC profile, an appropriate
 111 numerical scheme has to be proposed to solve the semiempirical transport equations of k and
 112 ε along with the continuity and momentum equations. The predicted SSC distribution based
 113 on the $k-\varepsilon$ turbulent model agrees well with experimental results, however, this numerical
 114 model requires considerable computation and can not directly reflect which physical quantity
 115 affects the sediment concentration. Similarly, the hydro-thermo-ice-sediment dynamical
 116 model employed by Huang (2014) and Knack (2011) lacks brevity and requires considerable
 117 computation. This motivates the current work in which we develop a concise and precise
 118 analytical model for predicting the SSC distribution in the ice-covered channel flows.

119 **Table 1**

120 Some previous models concerning the SSC prediction in the ice-covered channel flows.

Models	Adopted hypothesis/approach	References
Analytical model	The two-layer hypothesis and Boussinesq's hypothesis	Knack and Shen, 2015; Sayre and Song, 1979
Numerical model	The hydro-thermo-ice-sediment dynamical model, and the $k-\varepsilon$ turbulent model	Huang, 2014; Knack, 2011; Krishnappan, 1983; Lau and Krishnappan, 1985

121 In this study, we present a novel analytical model to predict the vertical profile of the SSC
 122 for the steady uniform flow in the ice-covered alluvial channels. First, the analytical
 123 expression of the vertical turbulent mass transfer coefficient is obtained by utilizing the eddy

124 viscosity model applied to asymmetric turbulent flows proposed by Guo et al. (2017). In light
125 of the dimensional limitation of experimental facilities, the sediment fall velocity is certainly
126 affected by the wall boundary. Accordingly, a modified formula for the sediment fall velocity,
127 which considers the combined effects of the upper and lower boundaries, is then proposed.
128 By introducing the formulas of the turbulent mass transfer coefficient and the sediment fall
129 velocity into the Schmidt O'Brien equation, an analytical model is derived to calculate the
130 SSC distribution in the ice-covered channel flows. Subsequently, the analytical SSC model is
131 verified by available experimental data and the prediction accuracy of the model is assessed
132 by comparing the calculated SSC distributions in this study with those found in the literature.
133 Finally, the influences of the pivotal characteristic parameters on the SSC profile in the
134 ice-covered channel flows are investigated.

135 **2. Method**

136 The sediment transport in the ice-covered alluvial channel flows is more complicated than
137 the sediment conveyance in the open channel flows due to the effect of a floating ice cover.
138 On the one hand, the turbulent coherent vortex generated underside the ice cover interacts
139 with that induced by the channel bottom (Lotsari et al., 2019; Muste et al., 2000), which
140 enhances the disturbance intensity and affects the turbulent shear stress distribution. The
141 redistribution of the turbulent shear stress will certainly influence the turbulent mass
142 diffusivity and hence the vertical distribution of the SSC. On the other hand, the presence of
143 the floating ice cover increases the pressure at the ice-water interface that is equal to the
144 atmospheric pressure plus the weight of the ice column per unit area. Correspondingly, the
145 fall velocity of the suspended sediment particle is expected to be affected by the floating ice

146 cover. Therefore, this study focuses on the analytical exploration of the SSC in the
147 ice-covered alluvial channel flows.

148 **2.1 Formulation of the suspended sediment concentration**

149 For an ice-covered channel with a steady uniform flow field, if the sinking sediment flux
150 due to the submerged weight is balanced by the net floating upward sediment flux due to the
151 turbulent diffusion, the SSC profile will then reach an equilibrium in the vertical direction,
152 which is similar to that in the open channel flows. Based on the Schmidt O'Brien equation,
153 the governing equation of the SSC profile in the steady uniform flow field of the ice-covered
154 channels can be expressed as (Sayre and Song, 1979):

$$155 \quad \Gamma_z \frac{dC}{dz} + \omega_s C = 0, \quad (1)$$

156 where C denotes the suspended sediment concentration, in mg/l; Γ_z is the vertical turbulent
157 mass transfer coefficient of the sediment particles, in m^2/s ; ω_s is the sediment fall velocity, in
158 m/s; and z denotes the vertical coordinate, in m. By solving Eq. (1), one has:

$$159 \quad \frac{C}{C_a} = \exp\left(-\int_a^z \frac{\omega_s}{\Gamma_z} dz\right), \quad (2)$$

160 where C_a is a reference sediment concentration at the vertical level $z = a$ from the channel
161 bed bottom, in mg/l.

162 To obtain the analytical solution of the SSC, it is required to know the distribution patterns
163 of the vertical turbulent mass transfer coefficient Γ_z and the sediment fall velocity ω_s . The
164 turbulent mass transfer coefficient is usually related to the eddy viscosity ν_t and can be
165 described as (Krishnappan, 1983):

$$166 \quad \Gamma_z = \sigma \nu_t, \quad (3)$$

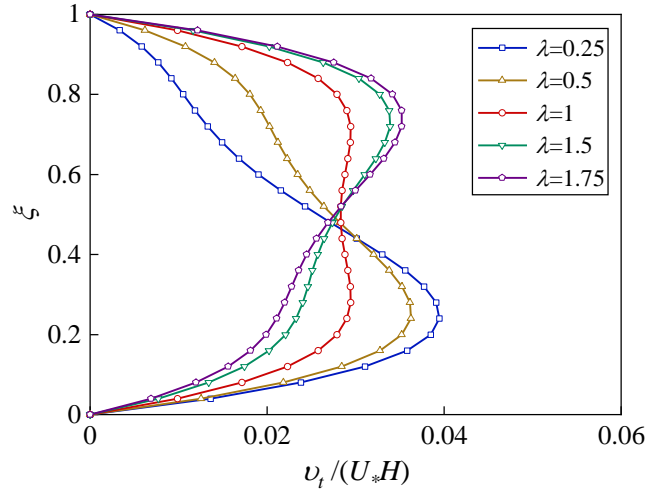
167 where σ is the dimensionless proportionality constant which is equal to the reciprocal of the
 168 turbulent Schmidt number. With regard to the eddy viscosity ν_t in the ice-covered channels,
 169 considering that there exist two sets of length and velocity scales for the turbulent mixing due
 170 to the different roughnesses between the channel bed and the ice cover, Guo et al. (2017)
 171 integrated the two scales into a single eddy viscosity equation and proposed an analytical
 172 model that can be applied to the asymmetric turbulent flow:

$$173 \quad \nu_t = 2\kappa H u_{*b} \beta \xi (1 - \xi) \left[1 + \alpha \left(\frac{\xi}{\xi_c} - 1 \right)^2 \right], \quad (4)$$

174 where κ is the von Kármán constant, and $\kappa = 0.40$; H is the total flow depth underneath the ice
 175 cover, in m; u_{*b} is the shear velocity of the lower bed layer, in m/s; $\beta = \frac{\lambda - \lambda^{2n}}{2(1 - \lambda^{2n})}$;

176 $\alpha = \frac{1 - \lambda}{\lambda - \lambda^{2n}}$; $\xi = \frac{z}{H}$; ξ_c represents the critical position of the eddy viscosity, and
 177 $\xi_c = \frac{1}{1 + \lambda^n}$ with $n = 5/6$; λ is a dimensionless parameter, and $\lambda = u_{*i}/u_{*b}$; and u_{*i} is the

178 shear velocity of the upper ice layer, in m/s. The vertical profile of the eddy viscosity ν_t can
 179 be attained if λ is known. Fig. 2 shows the eddy viscosity distribution with different λ values
 180 in the ice-covered channel flows. When $0 < \lambda < 1$, the shear velocity of the lower bed layer is
 181 greater than that of the upper ice layer and the turbulent coherent vortex due to the bed
 182 roughness dominates the turbulent mixing. When $\lambda = 1$, a symmetrical flow forms underneath
 183 the floating ice cover, and the turbulent coherent vortices generated by the bed roughness and
 184 the ice cover roughness are approximately equivalent in strength. When $\lambda > 1$, the turbulent
 185 coherent vortex of the upper ice layer plays a prominent role in the turbulent mixing.



186

187 **Fig. 2.** Vertical distributions of the eddy viscosity with different λ values in the ice-covered channel flows.

188 Substituting Eq. (4) into Eq. (3) yields the expression of the vertical turbulent mass transfer

189 coefficient Γ_z :

$$190 \quad \Gamma_z = 2\sigma\kappa H u_{*b} \beta \xi (1 - \xi) \left[1 + \alpha \left(\frac{\xi}{\xi_c} - 1 \right)^2 \right]. \quad (5)$$

191 Most studies on the fall velocity of the sediment particle assume that the water depth is

192 infinite, thereby introducing a constant sediment fall velocity throughout the flow depth.

193 However, the flow condition about the infinite water depth is impossible to achieve in

194 practice, especially in the laboratory experiment. When one studies the sediment settlement

195 law or the gradation analysis based on the sediment settlement law, the wall boundary of the

196 experimental facility will definitely affect the research results. Hence, it is necessary to take

197 into account the influence of the wall boundary on the sediment fall velocity. For an

198 ice-covered channel with shallow flows, the upper ice cover boundary and the lower channel

199 bed boundary will undoubtedly have an impact on the fall velocity of the sediment particle.

200 Hence, based on the work of Lorentz (1907), a modified formula for the sediment fall

201 velocity considering the influences of the upper ice cover and lower channel bed boundaries

202 is proposed as:

203
$$\omega_s = \frac{\omega_0}{1 + \varphi D/z} = \frac{\omega_0 \xi}{\xi + \varphi \xi_D}, \quad (6)$$

204 where ω_0 is the sediment fall velocity in the infinite flow field, in m/s; φ is the
 205 dimensionless correction coefficient that needs to be calibrated and its magnitude will affect
 206 the vertical distribution of the sediment fall velocity and hence the SSC profile; D is the
 207 median diameter of the sediment particle, in mm; z is the distance from the particle center to
 208 the channel bed, in m; and $\xi_D = D/H$. For the sediment fall velocity in the infinite flow field
 209 ω_0 , the formula proposed by Zhang (1998) is adopted:

210
$$\omega_0 = \sqrt{\left(13.95 \frac{\nu}{D}\right)^2 + 1.09 \frac{\gamma_s - \gamma_w}{\gamma_w} g D} - 13.95 \frac{\nu}{D}, \quad (7)$$

211 where ν is the kinematic viscosity coefficient of clear water, in m^2/s ; γ_s is the specific
 212 weight of sediment, in N/m^3 ; γ_w is the specific weight of clear water, in N/m^3 ; and g is the
 213 gravitational acceleration, in m/s^2 .

214 Accordingly, substituting Eqs. (5) and (6) into Eq. (2) yields:

215
$$\frac{C}{C_a} = \exp \left\{ - \frac{\omega_0}{2\sigma\kappa H u_{*b} \beta} \int_a^z \frac{1}{(1-\xi) \left[1 + \alpha \left(\frac{\xi}{\xi_c} - 1 \right)^2 \right] (\xi + \varphi \xi_D)} dz \right\}. \quad (8)$$

216 By dividing the integral term of Eq. (8) into partial fractions, we can get the exact expression
 217 of the integral term (see Appendix A1). Thus, the SSC in the ice-covered channel flows can
 218 be obtained as:

$$\begin{aligned}
C = C_a \exp \left\{ -\frac{\omega_0}{2\sigma\kappa u_{*b}\beta(1+\varphi\xi_D)} \left[\frac{\xi_c^2}{\alpha(1-\xi_c)^2 + \xi_c^2} \ln \frac{1-\xi_a}{1-\xi} + \frac{\xi_c^2}{\alpha(\varphi\xi_D + \xi_c)^2 + \xi_c^2} \ln \frac{\xi + \varphi\xi_D}{\xi_a + \varphi\xi_D} \right. \right. \\
+ \frac{\alpha\xi_c^2(\varphi\xi_D + 1)(\varphi\xi_D + 2\xi_c - 1)}{2(\alpha(1-\xi_c)^2 + \xi_c^2)(\alpha(\varphi\xi_D + \xi_c)^2 + \xi_c^2)} \ln \frac{\alpha(\xi - \xi_c)^2 + \xi_c^2}{\alpha(\xi_a - \xi_c)^2 + \xi_c^2} \\
\left. \left. + \frac{\sqrt{\alpha}\xi_c(\varphi\xi_D + 1)(\alpha(1-\xi_c)(\varphi\xi_D + \xi_c) + \xi_c^2)}{(\alpha(1-\xi_c)^2 + \xi_c^2)(\alpha(\varphi\xi_D + \xi_c)^2 + \xi_c^2)} \tan^{-1} \frac{\sqrt{\alpha}\xi_c(\xi - \xi_a)}{\xi_c^2 + \alpha(\xi - \xi_c)(\xi_a - \xi_c)} \right] \right\} \quad , (9)
\end{aligned}$$

where ξ_a is a dimensionless parameter, and $\xi_a = a/H$. If the correction coefficient $\varphi=0$ (i.e., $\omega_s = \omega_0$), the expression of the SSC that ignores the effect of the upper ice cover and lower channel bed boundaries on the sediment fall velocity is reduced to:

$$\begin{aligned}
C = C_a \exp \left\{ -\frac{\omega_0}{2\sigma\kappa u_{*b}\beta} \left[\frac{\xi_c^2}{\alpha(1-\xi_c)^2 + \xi_c^2} \ln \frac{1-\xi_a}{1-\xi} + \frac{1}{\alpha+1} \ln \frac{\xi}{\xi_a} \right. \right. \\
+ \frac{\alpha(2\xi_c - 1)}{2(\alpha+1)[\alpha(1-\xi_c)^2 + \xi_c^2]} \ln \frac{\alpha(\xi - \xi_c)^2 + \xi_c^2}{\alpha(\xi_a - \xi_c)^2 + \xi_c^2} \\
\left. \left. + \frac{\sqrt{\alpha}[\alpha(1-\xi_c) + \xi_c]}{(\alpha+1)[\alpha(1-\xi_c)^2 + \xi_c^2]} \tan^{-1} \frac{\sqrt{\alpha}\xi_c(\xi - \xi_a)}{\xi_c^2 + \alpha(\xi - \xi_c)(\xi_a - \xi_c)} \right] \right\} \quad . \quad (10)
\end{aligned}$$

2.2 Calibration of coefficients

In order to apply Eq. (9) to compute the SSC for an ice-covered channel, one requires to know the values of the shear velocity of the lower bed layer u_{*b} , the shear velocity of the upper ice layer u_{*i} , the dimensionless characteristic parameter λ , the reference sediment concentration C_a , the dimensionless correction coefficient φ , and the proportionality constant σ . This section presents the determination procedure of these physical parameters in detail.

2.2.1 Dimensionless characteristic parameter λ and shear velocities u_{*b} and u_{*i}

When studying the ice-covered channel flow, the two-layer hypothesis is usually adopted to divide the flow underneath the floating ice cover into two pseudo-free-surface flows (Sayre

233 and Song, 1979; Teal et al., 1994). As shown in Fig. 1, the two layers correspond to the upper
 234 ice layer and the lower bed layer, and their interface locates at the position of the maximum
 235 streamwise velocity. The flow characteristics in the two layers are dominated by the
 236 roughnesses of the ice cover and the channel bed, respectively. The relationship between the
 237 flow depth of the lower bed layer and the total flow depth can be expressed as (Tsai and
 238 Ettema, 1994):

$$239 \quad \frac{h_b}{H} = \frac{m_i}{m_b + m_i}, \quad (11)$$

240 where h_b is the flow depth of the lower bed layer, namely the distance from the channel bed
 241 bottom to the plane of the maximum streamwise velocity, in m; m_b and m_i are the
 242 dimensionless parameters related to the channel bed roughness and the ice cover roughness,
 243 respectively. Tsai and Ettema (1994) gave the expressions of the parameters m_b and m_i as:

$$244 \quad m_b = \kappa (8/f_b)^{1/2}, \quad (12)$$

$$245 \quad m_i = \kappa (8/f_i)^{1/2}, \quad (13)$$

246 where f_b and f_i are the Darcy-Weisbach resistance factors of the lower bed layer and the upper
 247 ice layer, respectively. By combining the Chezy formula with the Manning formula, one can
 248 obtain the resistance factors f_b and f_i as:

$$249 \quad f_b = \frac{8gn_b^2}{R_b^{1/3}}, \quad (14)$$

$$250 \quad f_i = \frac{8gn_i^2}{R_i^{1/3}}, \quad (15)$$

251 where n_b and n_i are the Manning's roughness coefficients associated with the channel bed and
 252 the ice cover, respectively; R_b and R_i are respectively the hydraulic radiuses of the lower bed
 253 layer and the upper ice layer, in m. Considering that the relationship between R_b and R_i can be

254 presented by $R_b/R_i = n_b^{3/2}/n_i^{3/2}$ (Wang et al., 2020), the relationship between f_b and f_i based
 255 on Eqs. (14) and (15) can be expressed as:

$$256 \quad f_b/f_i = (n_b/n_i)^{3/2}. \quad (16)$$

257 Hence, substituting Eqs. (12), (13), and (16) into Eq. (11) yields:

$$258 \quad h_b = \frac{H}{1 + (n_i/n_b)^{3/4}}, \quad (17)$$

259 According to $h_i = H - h_b$, the flow depth of the upper ice layer h_i can be expressed as:

$$260 \quad h_i = \frac{H}{1 + (n_b/n_i)^{3/4}}. \quad (18)$$

261 Given that the flows in the upper ice layer and the lower bed layer are usually deemed as
 262 two pseudo-free-surface flows, the shear velocities u_{*b} and u_{*i} of the two layers can be
 263 obtained from the momentum balance, which is similar to the uniform open-channel flow
 264 (Lau and Krishnappan, 1985; Muste et al., 2000):

$$265 \quad u_{*b} = \sqrt{gSh_b}, \quad (19)$$

$$266 \quad u_{*i} = \sqrt{gSh_i}, \quad (20)$$

267 where S is the channel bed slope. Substituting Eqs. (17) and (18) into Eqs. (19) and (20)
 268 yields:

$$269 \quad u_{*b} = \sqrt{\frac{gSH}{1 + (n_i/n_b)^{3/4}}}, \quad (21)$$

$$270 \quad u_{*i} = \sqrt{\frac{gSH}{1 + (n_b/n_i)^{3/4}}}. \quad (22)$$

271 Therefore, in line with $\lambda = u_{*i}/u_{*b}$, the dimensionless characteristic parameter λ can be
 272 presented as:

$$273 \quad \lambda = (n_i/n_b)^{3/8}. \quad (23)$$

274 **2.2.2 Reference sediment concentration C_a**

275 The method proposed by van Rijn (1984b) is adopted here for estimating the reference
276 concentration C_a :

$$277 \quad C_a = 0.015 \frac{D_{50} T_*^{1.5}}{a D_*^{0.3}}, \quad (24)$$

278 where a is the reference level from the channel bed bottom and assumed to be equal to the
279 half of the bed form height Δ (i.e., $a = 0.5\Delta$) while the bed form dimensions are known, or
280 else a is equal to the equivalent roughness height k_s (i.e., $a = k_s$), and a must satisfy $a \geq 0.01H$;
281 D_{50} is the particle median diameter of the bed material, in mm; D_* is a dimensionless
282 particle parameter, and $D_* = D_{50} [(s-1)g/v^2]^{1/3}$; s ($s = \rho_s/\rho$) is the dimensionless specific
283 density of the sediment particle; T_* is a dimensionless transport stage parameter. According
284 to the studies of Knack and Shen (2015) and van Rijn (1984a), the parameter T_* is defined
285 as:

$$286 \quad T_* = \left[\left(u_*' \right)^2 - \left(u_{*,cr} \right)^2 \right] / \left(u_{*,cr} \right)^2, \quad (25)$$

287 in which u_*' ($u_*' = \sqrt{\tau_b'/\rho}$) is the shear velocity related to the sediment particles, in m/s;
288 τ_b' ($\tau_b' = \gamma (n_b')^2 \bar{u}^2 / (\zeta_b H)^{1/3}$) is the bed shear stress related to the sediment particles, in N/m²;
289 n_b' ($n_b' = D_{50}^{1/6} / 20$) is the bed Manning's roughness coefficient related to the sediment
290 particles; \bar{u} is the mean streamwise velocity of the cross-section, in m/s; ζ_b ($\zeta_b = h_b/H$)
291 is the fraction of the flow depth influenced by the channel bed roughness; $u_{*,cr}$ is the critical
292 bed shear velocity, in m/s, which can be computed based on the Shields curve (as shown in
293 Fig. 1 of van Rijn, 1984a).

294 Note that the reference concentration C_a computed by Eq. (24) is in terms of solids volume

295 per unit fluid volume, and the unit of C_a can be transformed into kg/m^3 after multiplying by
 296 the sediment density ρ_s .

297 **2.2.3 Dimensionless correction coefficient φ and proportionality constant σ**

298 In this study, the correction coefficient of the sediment fall velocity φ and the
 299 proportionality constant σ are two free characteristic parameters and need to be empirically
 300 calibrated for computing the best fit with the available experimental suspended sediment
 301 concentration.

302 From the above analysis, if the values of u_{*b} , u_{*i} , λ , and C_a have been calculated and the
 303 values of φ and σ have been given, the SSC profile in an ice-covered channel can be
 304 computed by using Eq. (9). To clearly show the physical parameters required for the
 305 calculation of the SSC, we summarize the classification of these physical quantities in Table
 306 2.

307 **Table 2**

308 Physical parameters required for the calculation of the SSC in an ice-covered channel.

Parameters	Symbols
Measured parameters	D_{50} , q , H , S , Δ , ρ_s , T , n_i , and n_b
Calculated parameters	ω_0 calculated from Eq. (7), h_b calculated from Eq. (17), h_i calculated from Eq. (18), u_{*b} calculated from Eq. (21), u_{*i} calculated from Eq. (22), λ calculated from Eq. (23), a taken as $a = 0.5\Delta$, C_a calculated from Eq. (24), ξ_a calculated from $\xi_a = a/H$, ξ_c calculated from $\xi_c = 1/(1 + \lambda^n)$, ξ_D calculated from $\xi_D = D/H$, α calculated from $\alpha = (1 - \lambda)/(\lambda - \lambda^{2n})$, and β calculated from $\beta = (\lambda - \lambda^{2n})/(2(1 - \lambda^{2n}))$

309 **3. Results**

310 This section consists of two parts: the validation of the proposed SSC model and the
311 effects of the characteristic parameters on the SSC profile. When demonstrating the
312 effectiveness of the proposed SSC model, we employ the experimental data published in the
313 literature and calibrate the values of the correction coefficient φ and the proportionality
314 constant σ to improve the simulation accuracy. A series of values for the correction coefficient
315 φ , the proportionality constant σ , and the dimensionless characteristic parameters λ are
316 provided and the influences of these characteristic parameters on the SSC profile are
317 investigated.

318 **3.1 Comparison with experimental data**

319 The proposed SSC model is validated by comparing the simulated results with the
320 measured data from sediment transport experiments on the ice-covered channel flows
321 reported in the literature. These experiments included both the smooth and rough ice cover.
322 The detailed experimental conditions of the eight runs by Sayre and Song (1979) (notated
323 with AS, AR, BS, and BR), Lau and Krishnappan (1985) (represented as 4C, 5C, and 7C),
324 and Muste et al. (2000) (denoted as SC) are shown in Table 3. A brief description of these
325 experimental schemes is presented here for completeness and convenience.

326 Sayre and Song (1979) performed sediment transport experiments in a recirculating flume
327 with a sand bed and a simulated floating ice cover. The measuring section had glass-sided
328 walls and was 27.4 m long, 0.914 m wide, and 0.45 m deep. The flume slope could be
329 adjusted without interfering with the operation of the flume. The channel bed consisted of

330 quartz foundry sand with a median diameter of 0.25 mm and a geometric standard deviation
331 of 1.41. The simulated ice cover was composed of two types, namely smooth ice cover and
332 rough ice cover. To simulate the smooth ice cover, the adopted painted plywood panels,
333 which were 1.22 m in length, 0.91 m in width, and 1.27 cm in thickness, were connected by
334 hinges and formed a nonrigid floating cover expanding over almost the entire measuring
335 section. For constituting a rough ice cover, the 0.64 cm thick and 2.54 cm wide continuous
336 masonite strips were tacked to the undersurface of the panels with intervals of 15.24 cm.
337 Details of the experimental parameters are summarized in columns two to five in Table 3.

338 Lau and Krishnappan (1985) conducted the experiments in a rectangular flume with a
339 length of 57.3 m, a width of 0.756 m, and a depth of 0.29 m. The bed material was made up
340 of Flex-O-Lite BT10 glass beads with a median diameter of 0.15 mm and a specific gravity
341 of 2.50. The simulated ice cover consisted of 1.9 cm thick plywood panels whose underside
342 was glued by plastic laminate, thereby forming a very smooth bottom surface. For Runs 4C,
343 5C, and 7C, the channel slope was held constant as 0.001, while the flow discharge was
344 varied from 0.0154 m³/s to 0.0274 m³/s. Other flow parameters were listed in Table 3.

345 The sediment recirculating flume with a floating ice cover used by Muste et al. (2000) was
346 30 m long, 0.91 m wide, and 0.45 m deep. The flume slope was set to 1.5×10^{-4} with a
347 resolution of 5×10^{-4} . The flow discharge was kept constant at 0.0318 m³/s with an uncertainty
348 of 5×10^{-5} m³/s. The sediment bed was comprised of a uniform fine sand with a median
349 diameter of 0.25 mm, a geometric standard deviation of 1.4, and a specific gravity of 2.64.
350 The floating ice cover was simulated using 1.22 m long, 0.9 m wide, and 1.3 cm thick
351 plywood panels. Similar to the experiments of Sayre and Song (1979), the smooth ice cover

352 was formed by painting the underside surface of the panels, and the rough ice cover was
 353 modeled by gluing rectangular shaped wooden strips on the undersurface of the panels. We
 354 first utilize the experimental data with the smooth ice cover to carry out the simulation and
 355 comparison.

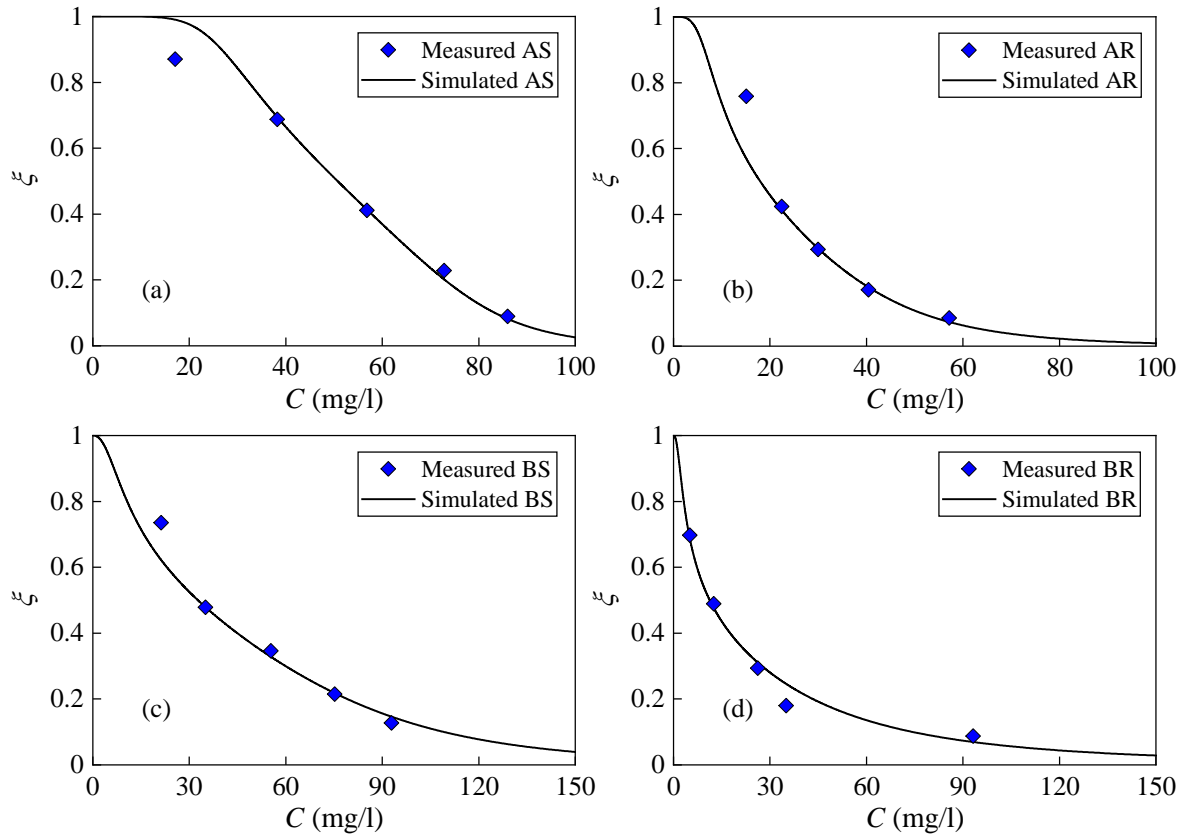
356 **Table 3**

357 Flow conditions of the ice-covered channel experiments and relevant parameters used in modeling the SSC
 358 profile.

Run	AS	AR	BS	BR	4C	5C	7C	SC
q (m ² /s)	0.0355	0.0332	0.0392	0.0428	0.0204	0.0266	0.0362	0.0349
H (m)	0.1180	0.1210	0.1220	0.1480	0.0877	0.0976	0.1160	0.1220
D_{50} (mm)	0.25	0.25	0.25	0.25	0.15	0.15	0.15	0.25
S (-)	1.80×10^{-3}	1.80×10^{-3}	2.04×10^{-3}	2.11×10^{-3}	1.00×10^{-3}	1.00×10^{-3}	1.00×10^{-3}	0.15×10^{-3}
γ_s (N/m ³)	2.6×10^4	2.6×10^4	2.6×10^4	2.6×10^4	2.45×10^4	2.45×10^4	2.45×10^4	2.59×10^4
γ_w (N/m ³)	9.8×10^3	9.8×10^3	9.8×10^3	9.8×10^3	9.8×10^3	9.8×10^3	9.8×10^3	9.8×10^3
T (°C)	16.9	20.5	19.7	18.2	20	20	20	20
Δ (cm)	1.84	1.59	2.01	1.76	1.16	1.33	1.30	4.00
n_i (-)	0.0114	0.0249	0.0108	0.0322	0.0090	0.0090	0.0090	0.0090
n_b (-)	0.0294	0.0228	0.0306	0.0236	0.0225	0.0225	0.0225	0.0225
φ (-)	1.2	1.0	1.3	1.1	0.8	1.2	1.0	1.1
σ (-)	16.7	9.3	6.6	4.3	1.5	1.1	1.3	6.0

359 Fig. 3 is the comparison between the simulated and the measured (Sayre and Song, 1979)
 360 SSC profile, where the simulated parameters φ and σ are empirically calibrated and listed in

361 Table 3. Overall, the simulated SSC profiles agree fairly well with the experimental results
362 for the four runs. It is also seen that near the ice cover bottom, the proposed SSC model
363 slightly overpredicts the SSC for Run AS and underpredicts the SSC for Runs AR and BS.
364 The correction coefficient of the sediment fall velocity φ for the four runs fluctuates around
365 1.15, which is larger than the value of 9/16 proposed by Lorentz (1907) in studying the
366 impact of the bottom horizontal boundary on the particle fall velocity. The values of the
367 proportionality parameter σ using in the simulation are relatively large and range from 4.3 to
368 16.7. In the study of Sayre and Song (1979), they also found unreasonably large values for
369 the proportionality parameter σ that ranged from 1.9 to 25. Sayre and Song (1979) ascribed
370 the unreasonable value of σ to the inaccurate measurement of the suspended sediment with a
371 moderately small quantity in the samples and also to the possibility that the adopted fall
372 velocity corresponding to the sediment median diameter was considerably greater than the
373 actual fall velocity of the suspended sediment. However, the relatively large value of σ
374 presented here may be related to the strength of the turbulent diffusion effect in the
375 experimental flow, which will be understood from the dependence of the SSC profile on the
376 proportionality parameter σ described in the next section.



377

378

Fig. 3. Comparison of the simulated and measured (Sayre and Song, 1979) SSC profile.

379

380

381

382

383

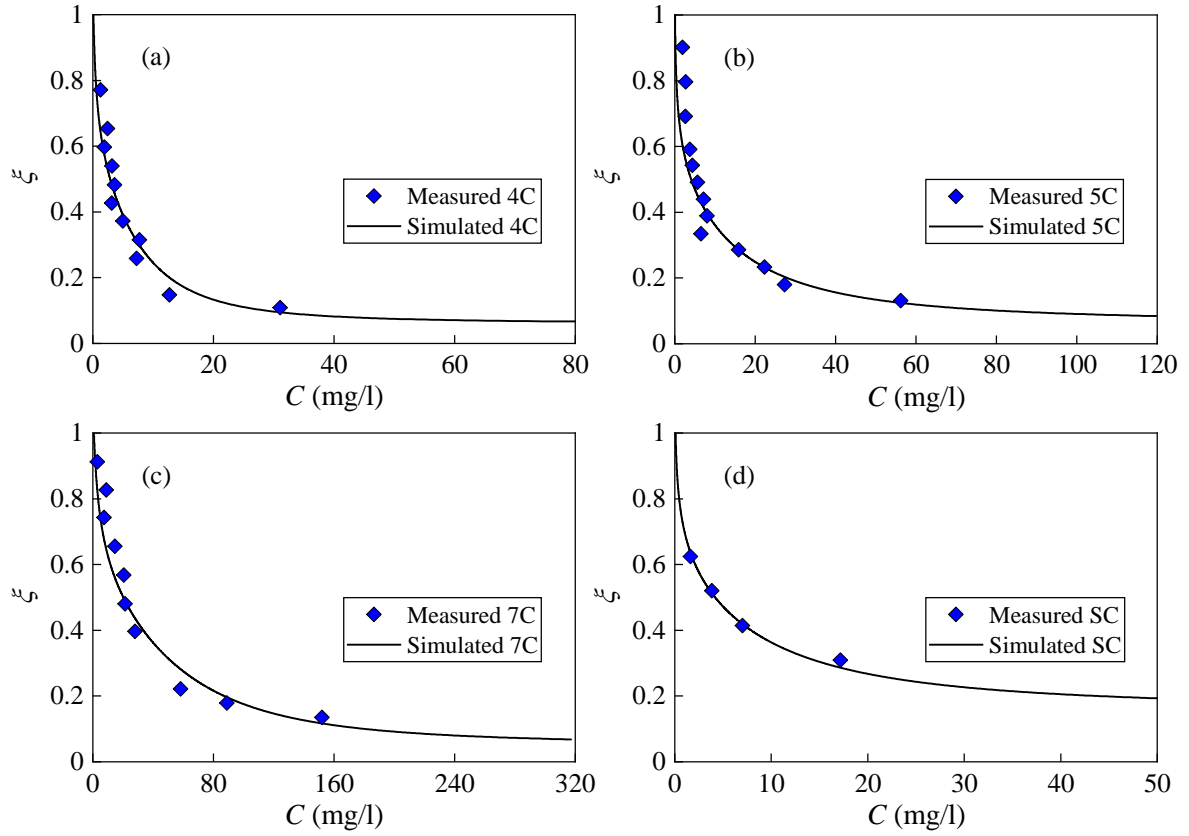
384

385

386

387

Fig. 4 shows the comparison of the simulated SSC profile with the experimental data from Lau and Krishnappan (1985) and Muste et al. (2000). From the visualization perspective, the proposed SSC model can provide a good prediction in the SSC distribution. It is noted that the proposed model slightly underestimates the SSC in the upper ice layer for Runs 4C, 5C, and 7C, which is similar to the simulation results in Runs AR and BS. This phenomenon may be ascribed to the fact that two turbulent coherent vortices appear beneath the ice cover, enhancing the SSC near the ice cover. Moreover, the averaged value of the proportionality parameter σ used in the simulation for Runs 4C, 5C, and 7C is 1.3 that is close to that used in the study of Lau and Krishnappan (1985).



388

389 **Fig. 4.** Comparison of the simulated SSC profile with experimental data from Lau and Krishnappan (1985)

390

and Muste et al. (2000).

391

To quantify the accuracy of the predicted SSC by the proposed model, error statistics for

392

the eight runs are carried out and shown in Table 4. The mean absolute error (*MAE*) is defined

393

as the average value of the difference between the computed and measured suspended

394

sediment concentrations:

395

$$MAE = \frac{1}{N} \sum_{i=1}^N |C_{com,i} - C_{mea,i}|, \quad (26)$$

396

where N is the sampling number of the measured suspended sediment concentrations for each

397

Run, C_{com} denotes the computed SSC using the proposed model, and C_{mea} represents the

398

measured SSC. The mean relative error (*MRE*) is expressed as:

399
$$MRE = \frac{1}{N} \sum_{i=1}^N \frac{|C_{com,i} - C_{mea,i}|}{C_{mea,i}} \quad (27)$$

400 Table 4 shows that the proposed analytical model simulates the SSC profiles within 3.34
 401 mg/l accuracy as far as the *MAE* is concerned, whereas the *MAE* values for Runs BR and 7C
 402 exceed 5.53 mg/l and 7.89 mg/l, respectively. The *MRE* ranges from 0.0836 to 0.1442 except
 403 for Runs 4C, 5C, and 7C whose *MRE* values reach up to 0.3567. The comparatively large
 404 values of the *MRE* for Runs 4C, 5C, and 7C are mainly caused by the underpredicted SSC in
 405 the upper ice layer. In the study of Lau and Krishnappan (1985), they ascribed the
 406 underpredicted results to the suspension of the finer fractions of the bed materials.

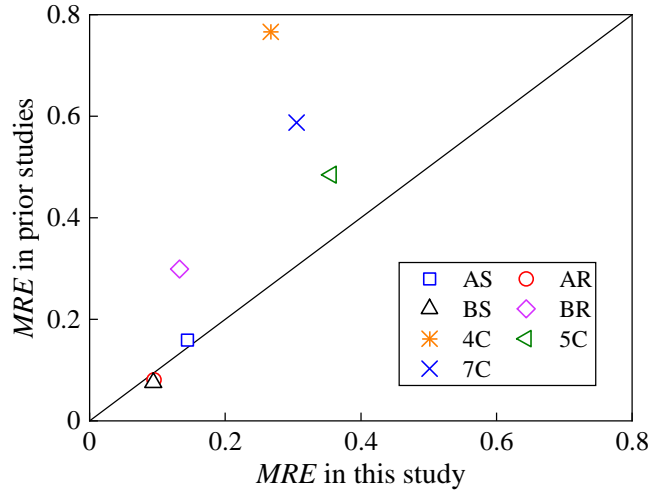
407 **Table 4**

408 Error statistics of the suspended sediment concentration for all Runs.

Run	AS	AR	BS	BR	4C	5C	7C	SC
<i>MAE</i> (mg/l)	3.0634	2.0113	3.3347	5.5340	1.6657	2.0655	7.8943	0.8260
<i>MRE</i> (-)	0.1442	0.0949	0.0941	0.1328	0.2669	0.3567	0.3054	0.0836

409 Krishnappan (1983) utilized the experimental data of Sayre and Song (1979) to predict the
 410 SSC profile, while Lau and Krishnappan (1985) also gave the modeled results for their
 411 measured suspended sediment concentrations. Accordingly, to evaluate the performance of
 412 the proposed SSC model in this study, the *MRE* calculated in this study is compared with that
 413 computed by Krishnappan (1983) and Lau and Krishnappan (1985), respectively. The result
 414 is shown in Fig. 5. For Runs AS, AR, and BS, the *MRE* in this study is approximately
 415 equivalent to the *MRE* in the previous studies. However, the *MRE* in this study is
 416 significantly smaller than the *MRE* in prior studies for other Runs. This demonstrates that the
 417 analytical SSC model presented in this study has higher accuracy than the model proposed by

418 Krishnappan (1983) and Lau and Krishnappan (1985).



419

420 **Fig. 5.** Comparison of the *MRE* in this study with the *MRE* in previous studies.

421 **3.2 Effect of characteristic parameters on the SSC**

422 In this section, the effect of the characteristic parameters λ , φ , and σ on the SSC
 423 distribution for the ice-covered channel flows has been studied using the validated analytical
 424 model. The vertical reference level adopted in simulations follows the convention and is
 425 selected as $0.05H$. Other parameters are listed in Table 5.

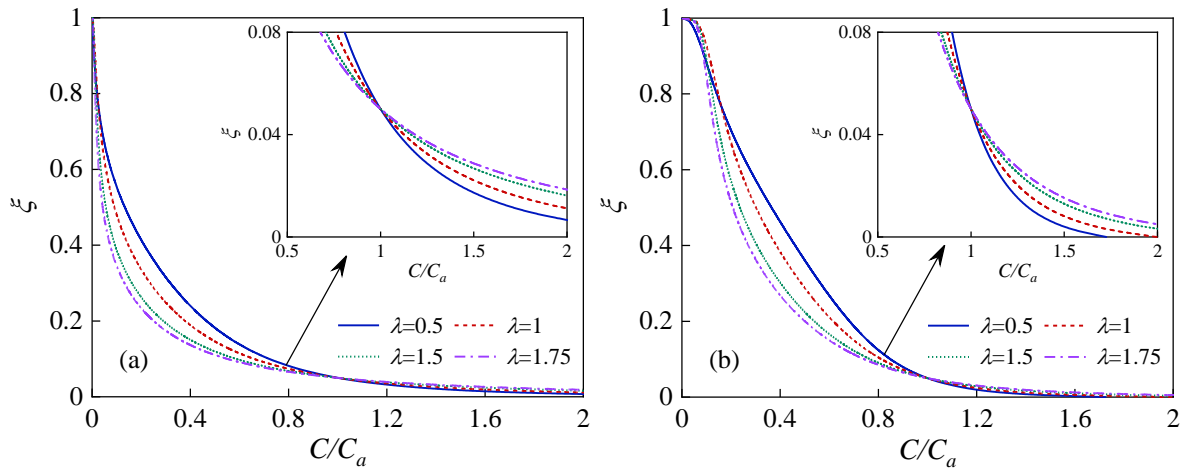
426 **Table 5**

427 Parameters used in the simulation for Figs. 6-8.

Figure	H (m)	D (mm)	S (-)	γ_s (N/m ³)	γ_w (N/m ³)	ν (m ² /s)	λ (-)	φ (-)	σ (-)
6	0.10	0.25	0.002	2.6×10^4	9.8×10^3	1.007×10^{-6}	0.5-1.75	1.5	5-10
7	0.10	0.25	0.002	2.6×10^4	9.8×10^3	1.007×10^{-6}	1.0	0.5-15	5-10
8	0.10	0.25	0.002	2.6×10^4	9.8×10^3	1.007×10^{-6}	1.0	1.5	0.5-20

428 Fig. 6 shows the influence of the characteristic parameter λ on the vertical distribution of
 429 the relative concentration of the suspended sediment C/C_a in an ice-covered channel with
 430 $\sigma=5$ and $\sigma=10$ (more detailed results with different values of σ are shown in Fig. A1 in the
 431 Appendix A). For a given value of σ , no matter what the value of λ is, the relative

432 concentration is very small near the bottom surface of the ice cover. This is similar to the
 433 situation of the free-surface flows. At a given elevation satisfying $\zeta > \zeta_a$, the relative
 434 concentration decreases with the increase of λ ; whereas the relative concentration increases as
 435 λ increases for a given elevation satisfying $\zeta < \zeta_a$. Thus, the smaller the value of λ is, the more
 436 uniform the concentration distribution is. This means that, under the same channel bed
 437 roughness, the relatively small ice cover roughness is conducive to suspending the sediment
 438 particle. These results are consistent with the research of Krishnappan (1983), who presented
 439 a series of concentration distribution curves with different ratios of the ice cover roughness to
 440 the channel bed roughness.

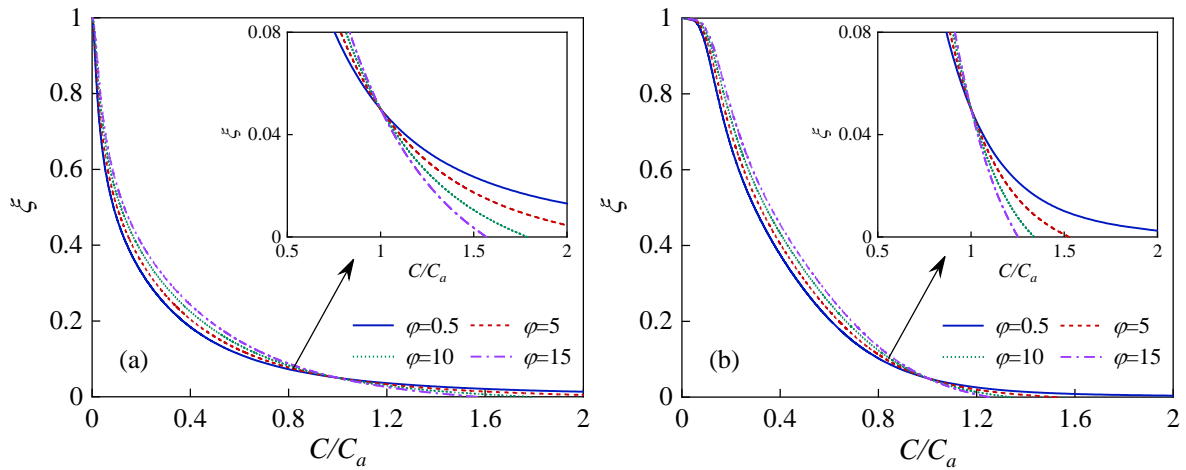


441
 442 **Fig. 6.** Effect of the parameter λ on the concentration distribution for different conditions. (a) $\sigma = 5$, $\varphi = 1.5$;

443 (b) $\sigma = 10$, $\varphi = 1.5$.

444 The impact of the correction coefficient φ on the simulated distribution of the relative
 445 concentration in an ice-covered channel with $\sigma=5$ and $\sigma=10$ is presented in Fig. 7 (more
 446 detailed results with different values of σ are shown in Fig. A2 in the Appendix A). It can be
 447 seen that the relative concentration has a similar variation trend as φ changes for different
 448 values of σ . When $\zeta > \zeta_a$, the value of the relative concentration is greater for larger values of

449 the correction coefficient φ , suggesting that the smaller the sediment fall velocity is, the
 450 larger the relative concentration is, which coincides with the physical mechanism.
 451 Nevertheless, the relative concentration presents a negative correlation with the increase of φ
 452 for $\zeta < \zeta_a$. Note that the variation law of the relative concentration induced by different values
 453 of φ is opposite to that created by diverse values of λ . Meanwhile, by comparing Fig. 6 with
 454 Fig. 7, the concentration profile is more sensitive to the parameter λ , which means that the
 455 impact of the varying upper and lower boundary roughness on the concentration distribution
 456 is more noticeable than that of the changing sediment fall velocity on the concentration
 457 distribution.

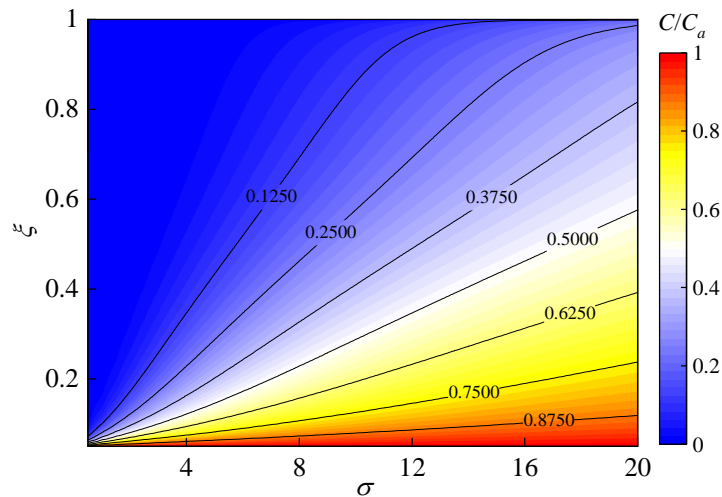


458
 459 **Fig. 7.** Effect of the parameter φ on the concentration distribution for different conditions. (a) $\sigma = 5, \lambda = 1$;

460 (b) $\sigma = 10, \lambda = 1$.

461 Fig. 8 presents the dependence of the concentration profile on the proportionality
 462 parameter σ when $\lambda = 1$ and $\varphi = 1.5$ (more detailed results with different values of λ and φ are
 463 shown in Figs. A3 and A4 in the Appendix A). At a given vertical elevation, the value of the
 464 relative concentration is greater for larger values of the proportionality parameter σ ,
 465 indicating that the proportionality parameter σ reflects the uniformity of the concentration

466 profile. In fact, the simulated results presented here can be explained from the perspective of
 467 the physical mechanism. According to Eq. (3), it is known that the larger the value of σ is, the
 468 more conspicuous the turbulent diffusion effect is. When the turbulent diffusion effect with a
 469 relatively large σ is much greater than the gravity effect, the sediment particles will be easily
 470 suspended in the water body, thereby generating a comparatively uniform concentration
 471 profile. Therefore, if the vertical profile of the relative concentration is known, it can be
 472 inferred the degree of the turbulent diffusion effect and hence the rough value of the
 473 proportionality parameter σ .



474
 475 **Fig. 8.** Dependence of the concentration distribution on the proportionality parameter σ with $\lambda = 1$ and $\varphi =$
 476 1.5.

477 4. Discussion

478 When an ice cover is formed on the channel flow surface, the boundary shear stress and the
 479 eddy viscosity corresponding to the lower bed layer of the ice-covered channel flows are both
 480 smaller than that corresponding to the bed boundary of the ice-free channel flows.
 481 Whereupon the ability of the flow to transport sediments is declined due to the reduced bed
 482 shear stress, leading to a decrease of SSC as well as the suspended sediment load. In light of

483 these facts, this study proposes an analytical SSC model based on the Schmidt O'Brien
484 equation. The proposed SSC model considers the effect of the additional ice cover on the
485 sediment fall velocity. An eddy viscosity model that can be applied to the ice-covered channel
486 flow is also employed in the derivation of the SSC model. The proposed SSC model is then
487 validated by comparing with the available sediment transport experiments on the ice-covered
488 channel flows reported in the literature. The accuracy of the proposed SSC model is evaluated.
489 Meanwhile, the effect of both the parameter λ and the sediment fall velocity correction
490 coefficient φ on the SSC is investigated by using the proposed model. Simulated results show
491 that the smaller ice cover roughness relative to the channel bed roughness is favorable to the
492 suspension of the sediment particles, and the SSC is more sensitive to the variation of the
493 boundary roughness than to the variation of the sediment fall velocity. Besides, it has been
494 found that there is a correlation between the uniformity of the concentration profile and the
495 magnitude of the proportionality parameter σ .

496 Although several models had been developed for predicting the suspended sediment
497 concentration for the ice-covered channel flows in previous studies, all these SSC models
498 were not concisely expressed as a straightforward equation. In the study of Sayre and Song
499 (1979), the turbulent mass transfer coefficient Γ_z near the lower and upper boundaries
500 followed the parabola distribution, whereas Γ_z in the middle flow depth zone was assumed to
501 be distributed linearly between the vertices of the lower and upper parabolas. Given that the
502 distribution of Γ_z in the central region was given without any theoretical foundation, the
503 reliability of the SSC model proposed by Sayre and Song (1979) needs further verification. In
504 the studies of Krishnappan (1983) and Lau and Krishnappan (1985), they obtained the

505 distribution of the eddy viscosity ν_t based on the $k-\varepsilon$ turbulent model and then developed the
506 profile of Γ_z utilizing the assumed proportional relationship between Γ_z and ν_t . The SSC
507 distribution curves for the ice-covered channel flows were then obtained by solving the
508 Schmidt O'Brien equation. However, the methods for predicting the SSC developed by
509 Krishnappan (1983) and Lau and Krishnappan (1985) are implicit and appropriate numerical
510 schemes are required for solving the $k-\varepsilon$ turbulent model involved.

511 Different from previous studies, the SSC model proposed in this study is expressed as an
512 explicit equation that can be easily computed by using MATLAB to investigate how the
513 characteristic parameters affect the SSC profile in the ice-covered channel flow. The
514 simulation results show that the proposed SSC model has higher accuracy than previously
515 reported methods in terms of the predicted SSC profile. However, there is still room for
516 improvement as the model underestimates the suspended sediment concentration near the
517 upper boundary. Note that, due to the limitation of available experimental data, the correction
518 coefficient of the sediment fall velocity φ used in the simulation for the eight runs in this
519 study fluctuates around the value of 1.09 which lacks the universality and may not apply to
520 other ice-covered flow conditions. Therefore, further sediment transport experiments in an
521 ice-covered channel are required to be conducted for investigating the general value for the
522 correction coefficient φ .

523 **5. Conclusions**

524 To obtain a thorough knowledge of the SSC profile for the ice-covered alluvial channels
525 with steady uniform flows, this study proposes an analytical SSC model by utilizing the eddy
526 viscosity model applied to the asymmetric turbulent flow and considering the common effects

527 of the upper and lower boundaries on the sediment fall velocity. The proposed model is
528 validated by comparing the simulated results with available experimental data. The validated
529 model is then used to investigate the effects of the characteristic parameters on the vertical
530 distribution of the SSC in the ice-covered channel. The following conclusions can be drawn
531 from this study:

532 (1) The agreement between the simulated SSC profile and the laboratory measured data
533 reported in the literature is satisfactory. Nonetheless, the simulated results underpredict
534 the SSC in the upper ice layer, which may be caused by the coherent vortex generating
535 underside the ice cover. The error statistics analysis illustrates that the performance of the
536 proposed model is better than previous models in terms of predicting the suspended
537 sediment concentration profile in the ice-covered channel flows.

538 (2) The relative suspended sediment concentration decreases as the parameter λ increases at
539 a given elevation satisfying $\zeta > \zeta_a$, while the relative concentration increases with the
540 increase of the parameter λ for $\zeta < \zeta_a$. As the parameter λ actually reflects the ratio of the
541 ice cover roughness to the channel bed roughness, it can be inferred that the sediment
542 particles are more likely to be suspended under the action of a smaller ice cover
543 roughness.

544 (3) The impact of the correction coefficient of the sediment fall velocity on the SSC
545 distribution is in contrast to the effect of the parameter λ on the SSC profile. Although the
546 relative concentration decreases as the ice cover roughness and the sediment fall velocity
547 increase, the boundary roughness has a relatively prominent influence on the relative
548 concentration profile.

549 (4) The simulated relative concentration profile becomes more uniform as the
 550 proportionality parameter σ increases. This result is consistent with the physical
 551 mechanism that the uniformity of the SSC profile is mainly determined by the strength of
 552 the turbulent diffusion effect, while the magnitude of the proportionality parameter σ
 553 actually represents the extent of the turbulent diffusion effect.

554 Although this study presents an effective analytical model to compute the SSC for the
 555 ice-covered alluvial channels, there are still some aspects that could be improved in future
 556 work. For example, the available laboratory measured data that can be found in the literature
 557 are limited, which restricts the detailed analysis and study of the sediment fall velocity
 558 correction coefficient φ that is very important in determining the SSC. Further experiments in
 559 the ice-covered sediment-laden flow are required in order to investigate the universal value or
 560 range of φ . Besides, given that numerical simulation is a significant tool for investigating the
 561 water and sediment transport process, the motion of sediment particles, such as the rolling
 562 and sliding motion, the saltation motion, and the suspended particle motion in the ice-covered
 563 channel flows could be simulated by utilizing the sophisticated numerical models.

564 **Appendix A**

565 **A1. Derivation of the analytical solution of the SSC**

566 In this part, the derivation process of Eq. (9) is illustrated in detail. For the sake of brevity,
 567 the integral term in Eq. (8) is labeled by I , namely

$$568 \quad I = \int_a^z \frac{1}{(1-\xi) \left[1 + \alpha \left(\frac{\xi}{\xi_c} - 1 \right)^2 \right] (\xi + \varphi \xi_D)} dz. \quad (\text{A1})$$

569 Thus, Eq. (8) can be rewritten as

570
$$\frac{C}{C_a} = \exp \left\{ -\frac{\omega_0}{2\sigma\kappa H u_{*b}\beta} \cdot I \right\}. \quad (\text{A2})$$

571 To obtain the integral result of the righthand side of Eq. (A1), I can be divided into partial
572 fractions and rearranged as:

573
$$I = \frac{H}{1 + \varphi_{\xi_D}^{\xi}} \int_{\xi_a}^{\xi} \left\{ \frac{1}{(1-\xi) \left[1 + \alpha \left(\frac{\xi}{\xi_c} - 1 \right)^2 \right]} + \frac{1}{\left[1 + \alpha \left(\frac{\xi}{\xi_c} - 1 \right)^2 \right] (\xi + \varphi_{\xi_D}^{\xi})} \right\} d\xi, \quad (\text{A3})$$

$$= \frac{H}{1 + \varphi_{\xi_D}^{\xi}} \int_{\xi_a}^{\xi} \left\{ a_0 \frac{1}{(1-\xi)} + b_0 \frac{1}{\xi + \varphi_{\xi_D}^{\xi}} + c_0 \frac{(2\alpha/\xi_c)(\xi/\xi_c - 1)}{1 + \alpha(\xi/\xi_c - 1)^2} + d_0 \frac{\sqrt{\alpha}/\xi_c}{1 + \alpha(\xi/\xi_c - 1)^2} \right\} d\xi$$

574 where

575
$$a_0 = \frac{1}{\alpha(1/\xi_c - 1)^2 + 1}, \quad b_0 = \frac{1}{\alpha(\varphi_{\xi_D}^{\xi}/\xi_c + 1)^2 + 1}, \quad c_0 = \frac{(\alpha/\xi_c^2)(\varphi_{\xi_D}^{\xi} + 1)(\varphi_{\xi_D}^{\xi} + 2\xi_c - 1)}{2 \left[\alpha(1/\xi_c - 1)^2 + 1 \right] \left[\alpha(\varphi_{\xi_D}^{\xi}/\xi_c + 1)^2 + 1 \right]},$$

576 and
$$d_0 = \frac{(\sqrt{\alpha}/\xi_c)(\varphi_{\xi_D}^{\xi} + 1) \left[\alpha(1/\xi_c - 1)(\varphi_{\xi_D}^{\xi}/\xi_c + 1) + 1 \right]}{\left[\alpha(1/\xi_c - 1)^2 + 1 \right] \left[\alpha(\varphi_{\xi_D}^{\xi}/\xi_c + 1)^2 + 1 \right]}.$$
 The integral result of the righthand

577 side of Eq. (A3) can then be easily obtained:

578
$$I = \frac{H}{1 + \varphi_{\xi_D}^{\xi}} \left[a_0 \ln \frac{1 - \xi_a}{1 - \xi} + b_0 \ln \frac{\xi + \varphi_{\xi_D}^{\xi}}{\xi_a + \varphi_{\xi_D}^{\xi}} + c_0 \ln \frac{1 + \alpha(\xi/\xi_c - 1)^2}{1 + \alpha(\xi_a/\xi_c - 1)^2} \right. \\ \left. + d_0 \tan^{-1} \frac{(\sqrt{\alpha}/\xi_c)(\xi - \xi_a)}{1 + \alpha(\xi/\xi_c - 1)(\xi_a/\xi_c - 1)} \right]. \quad (\text{A4})$$

579 Finally, substituting Eq. (A4) into Eq. (A2) yields the analytical solution of the SSC in the
580 ice-covered sediment-laden channel flow:

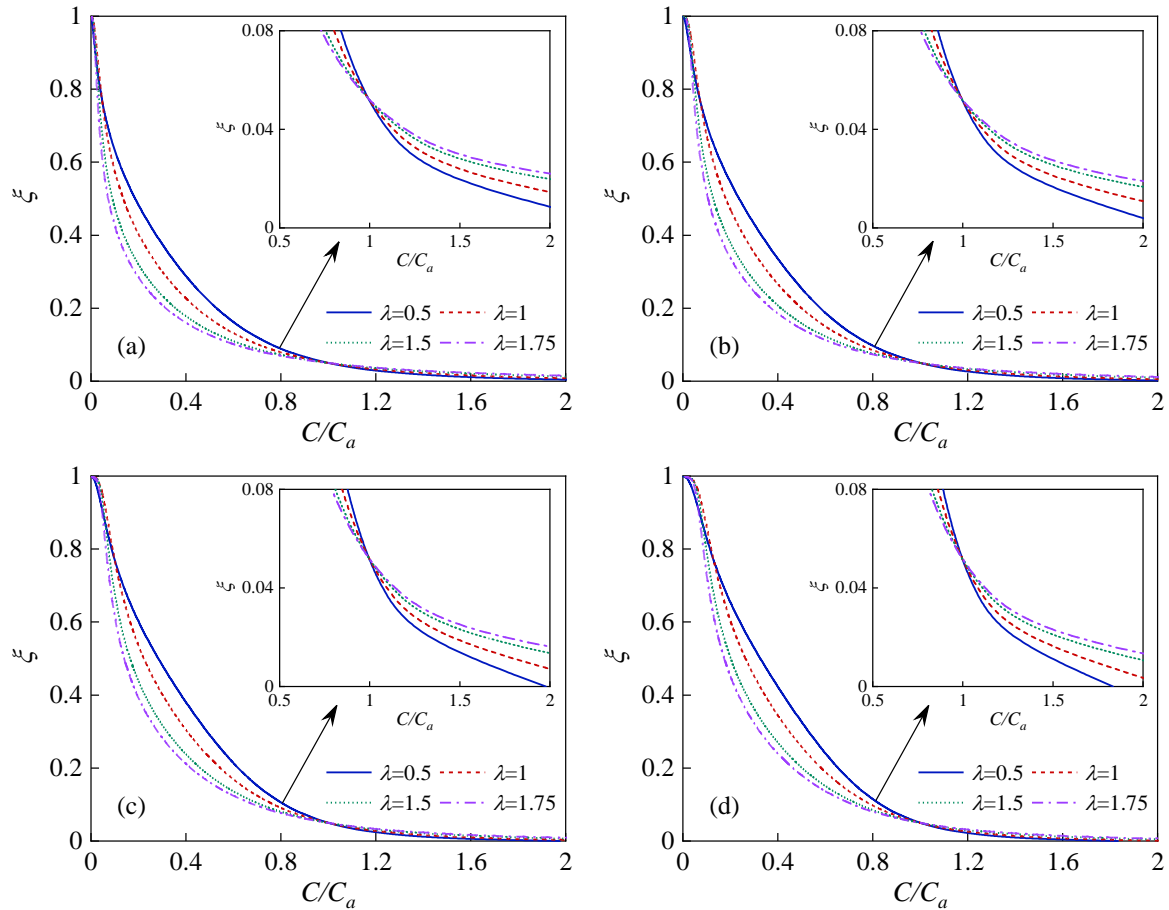
581
$$C = C_a \exp \left\{ -\frac{\omega_0}{2\sigma\kappa u_{*b}\beta(1 + \varphi_{\xi_D}^{\xi})} \left[a_0 \ln \frac{1 - \xi_a}{1 - \xi} + b_0 \ln \frac{\xi + \varphi_{\xi_D}^{\xi}}{\xi_a + \varphi_{\xi_D}^{\xi}} \right. \right. \\ \left. \left. + c_0 \ln \frac{1 + \alpha(\xi/\xi_c - 1)^2}{1 + \alpha(\xi_a/\xi_c - 1)^2} + d_0 \tan^{-1} \frac{(\sqrt{\alpha}/\xi_c)(\xi - \xi_a)}{1 + \alpha(\xi/\xi_c - 1)(\xi_a/\xi_c - 1)} \right] \right\}. \quad (\text{A5})$$

582 Eq. (A5) is exactly the same as Eq. (9) by substituting the expressions of a_0 , b_0 , c_0 , and d_0 into

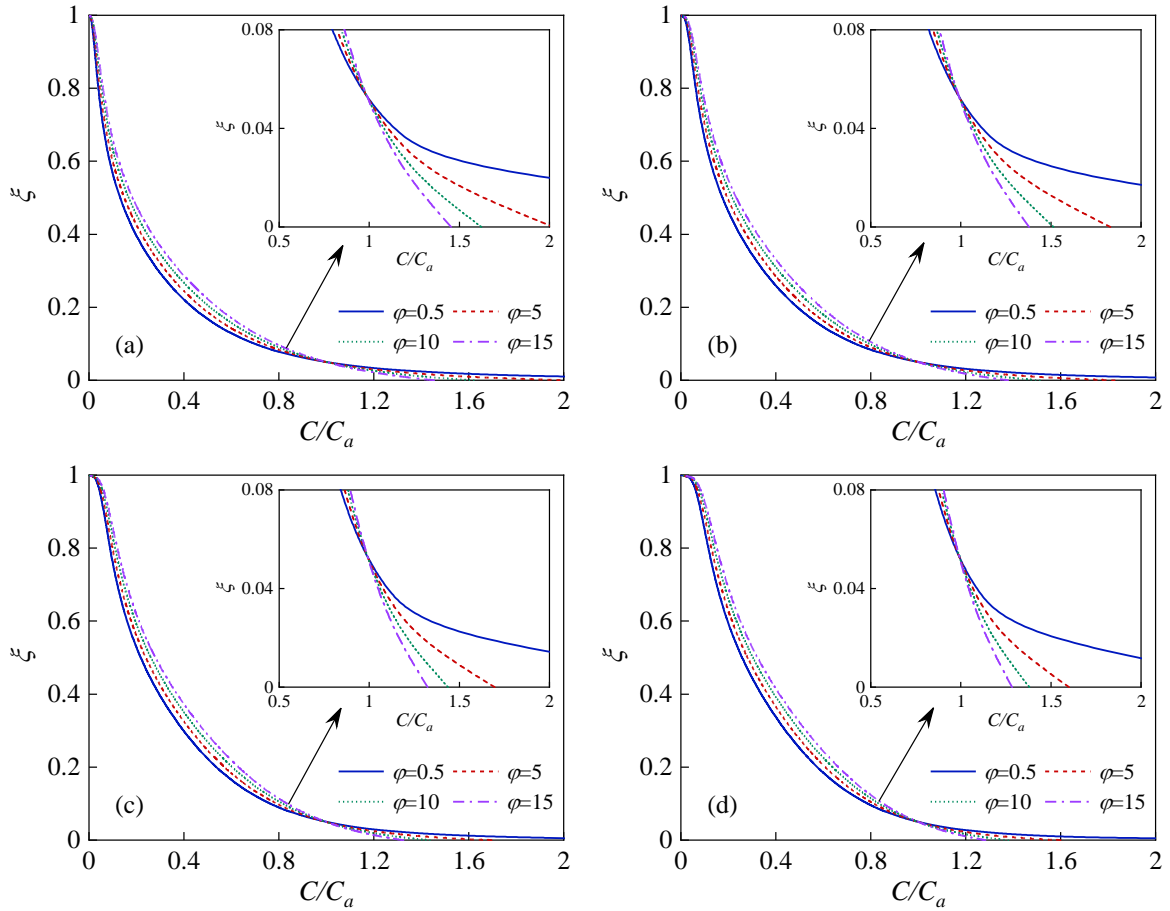
583 Eq. (A5).

584 **A2. Effect of λ , φ , and σ on the SSC**

585 In order to further illustrate the impact of the characteristic parameters λ , φ , and σ on the
 586 SSC distribution for the ice-covered channel flows, Figs. A1-A4 are shown as a supplement
 587 to Figs. 6-8.



588
 589 **Fig. A1.** Effect of the parameter λ on the concentration distribution for different conditions. (a) $\sigma = 6$, $\varphi =$
 590 1.5 ; (b) $\sigma = 7$, $\varphi = 1.5$; (c) $\sigma = 8$, $\varphi = 1.5$; (d) $\sigma = 9$, $\varphi = 1.5$.

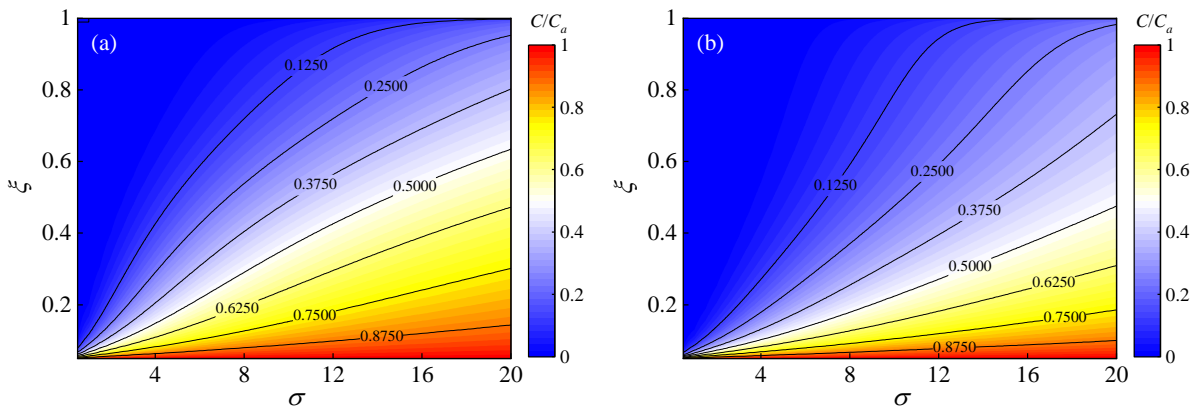


591

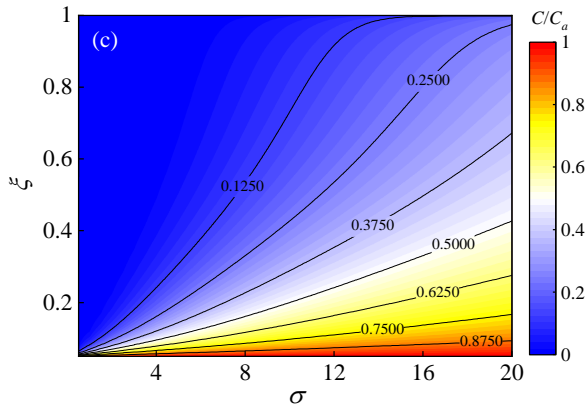
592 **Fig. A2.** Effect of the parameter φ on the concentration distribution for different conditions. (a) $\sigma = 6, \lambda = 1$;

593

(b) $\sigma = 7, \lambda = 1$; (c) $\sigma = 8, \lambda = 1$; (d) $\sigma = 9, \lambda = 1$.



594

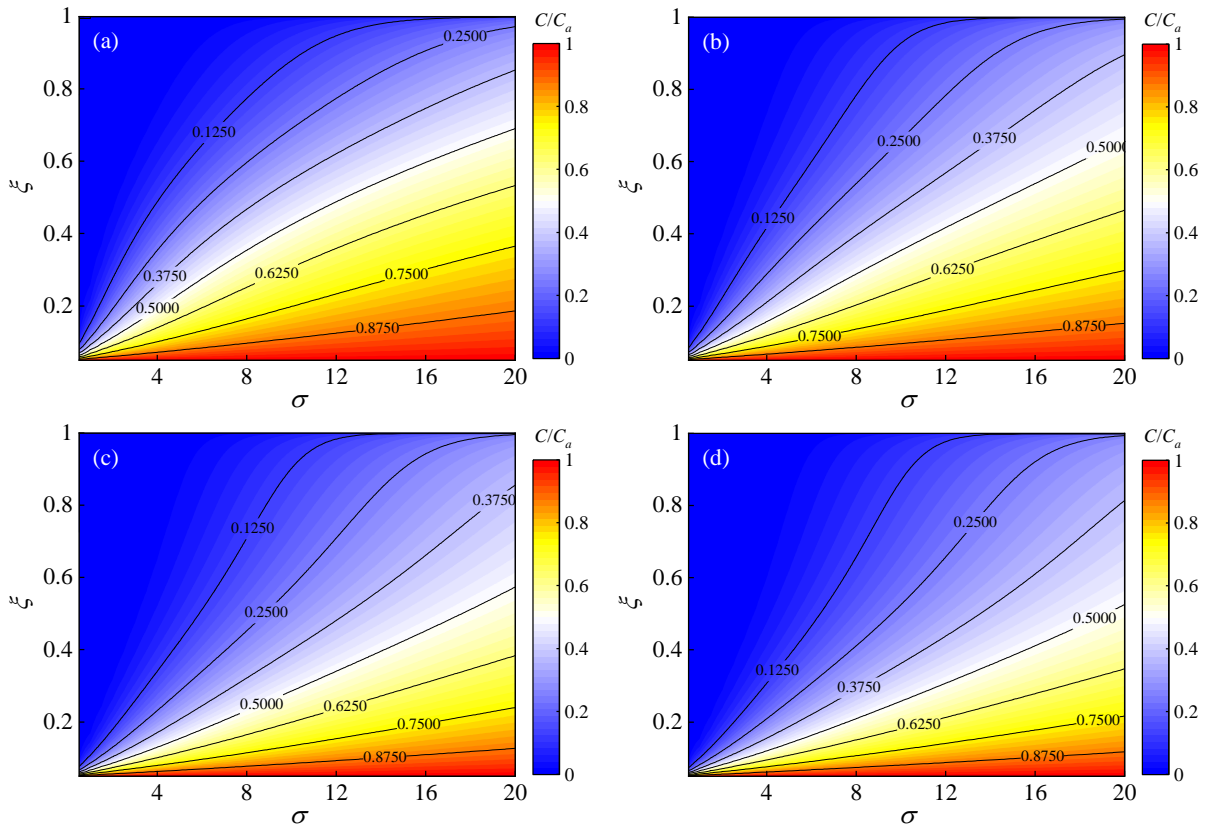


595

596 **Fig. A3.** Dependence of the concentration distribution on the proportionality parameter σ . (a) $\lambda = 0.5$, $\varphi =$

597

1.5; (b) $\lambda = 1.5$, $\varphi = 1.5$; (c) $\lambda = 1.75$, $\varphi = 1.5$.



598

599

600 **Fig. A4.** Dependence of the concentration distribution on the proportionality parameter σ . (a) $\lambda = 0.5$, $\varphi =$

601

15; (b) $\lambda = 1.0$, $\varphi = 15$; (c) $\lambda = 1.5$, $\varphi = 15$; (d) $\lambda = 1.75$, $\varphi = 15$.

602 Acknowledgements

603 This work was supported by the National Natural Science Foundation of China (grant

604 numbers 52020105006 and 11872285) and the Open Funding of State Key Laboratory of

605 Water Resources and Hydropower Engineering Science (WRHES), Wuhan University
606 (Project number 2018HLG01).

607 **Nomenclature**

608 *The following symbols are used in this paper:*

- a Reference level from the channel bed bottom (m)
- C Suspended sediment concentration (mg/l)
- C_a Reference sediment concentration at the vertical level $z = a$ from the channel bed bottom (mg/l)
- D_{50} Median diameter of the bed material (mm)
- D_* Dimensionless particle parameter (-)
- f_b Darcy-Weisbach resistance factor of the lower bed layer (-)
- f_i Darcy-Weisbach resistance factor of the upper ice layer (-)
- F_D Drag force exerted on the sediment particle (N)
- F_L Lift force due to the turbulent diffusion effect (N)
- g Gravitational acceleration (m/s^2)
- h_b Flow depth of the lower bed layer (m)
- h_i Flow depth of the upper ice layer (m)
- H Total flow depth (m)
- k_s Equivalent roughness height (m)
- m_b Parameter related to the channel bed roughness (-)
- m_i Parameter related to the ice cover roughness (-)
- n_b Manning's roughness coefficient associated with the channel bed (-)

n_i	Manning's roughness coefficient associated with the ice cover (-)
n_b'	Bed Manning's roughness coefficient related to sediment particles (-)
q	Flow discharge per unit width (m^2/s)
s	Dimensionless specific density of the sediment particle (-)
S	Channel bed slope (-)
T	Temperature of clear water ($^{\circ}\text{C}$)
T_*	Transport stage parameter (-)
\bar{u}	Mean streamwise velocity of the cross-section (m/s)
u_{*b}	Shear velocity of the lower bed layer (m/s)
u_{*i}	Shear velocity of the upper ice layer (m/s)
$u_{*,cr}$	Critical bed shear velocity (m/s)
u_*'	Shear velocity related to sediment particles (m/s)
U_{\max}	Maximum streamwise velocity (m/s)
W	Submerged weight of the sediment particle that is equal to the difference between the particle gravity and the buoyancy (N)
x	Streamwise coordinate (m)
z	Vertical coordinate (m)
κ	von Kármán constant, and $\kappa = 0.40$ (-)
σ	Proportionality constant (-)
ζ	Dimensionless parameter, and $\zeta = z/H$ (-)
ζ_a	Dimensionless parameter, and $\zeta_a = a/H$ (-)
ζ_c	Critical position of the eddy viscosity (-)

ζ_D	Dimensionless parameter, and $\zeta_D = D/H$ (-)
α, β	Intermediate parameters (-)
Γ_z	Turbulent mass transfer coefficient of sediment particle in the vertical direction (m^2/s)
ρ_s	Density of sediment (kg/m^3)
ρ	Density of clear water (kg/m^3)
γ_s	Specific weight of sediment, and $\gamma_s = \rho_s g$ (N/m^3)
γ_w	Specific weight of clear water, and $\gamma_w = \rho g$ (N/m^3)
ω_s	Fall velocity of sediment particle (m/s)
ω_0	Sediment fall velocity in the infinite flow field (m/s)
φ	Correction coefficient of sediment fall velocity (-)
ν	Kinematic viscosity coefficient of clear water (m^2/s)
ν_t	Eddy viscosity (m^2/s)
λ	Dimensionless parameter, and $\lambda = u_{*t}/u_{*b}$ (-)
Δ	Bed form height (cm)
τ_b'	Bed shear stress related to sediment particles (N/m^2)
τ_{zx}	Turbulent shear stress with respect to the horizontal plane (N/m^2)
ζ_b	Fraction of the flow depth influenced by the channel bed roughness (-)

609 **References**

- 610 Beltaos, S., Burrell, B.C., 2016. Transport of suspended sediment during the breakup of the ice cover,
611 Saint John River, Canada. Cold Reg. Sci. Tech. 129, 1-13.
612 <https://doi.org/10.1016/j.coldregions.2016.05.006>.

613 Brayshaw, A.C., Frostick, L.E., Reid, I., 1983. The hydrodynamics of particle clusters and sediment
614 entrainment in coarse alluvial channels. *Sedimentology* 30 (1), 137-143.
615 <https://doi.org/10.1111/j.1365-3091.1983.tb00656.x>.

616 Caissie, D., Kurylyk, B.L., St-Hilaire, A., El-Jabi, N., MacQuarrie, K.T.B., 2014. Streambed temperature
617 dynamics and corresponding heat fluxes in small streams experiencing seasonal ice cover. *J. Hydrol.*
618 519, 1441-1452. <https://doi.org/10.1016/j.jhydrol.2014.09.034>.

619 Cellino, M., Lemmin, U., 2004. Influence of coherent flow structures on the dynamics of suspended
620 sediment transport in open-channel flow. *J. Hydraul. Eng.* 130 (11), 1077-1088.
621 [https://doi.org/10.1061/\(ASCE\)0733-9429\(2004\)130:11\(1077\)](https://doi.org/10.1061/(ASCE)0733-9429(2004)130:11(1077)).

622 Chassiot, L., Lajeunesse, P., Bernier, J.F., 2020. Riverbank erosion in cold environments: Review and
623 outlook. *Earth-Sci. Rev.* 207, 103231. <https://doi.org/10.1016/j.earscirev.2020.103231>.

624 Cheng, N.S., Wei, M.X., Lu, Y.S., 2020. Critical flow velocity for incipient sediment motion in open
625 channel flow with rigid emergent vegetation. *J. Eng. Mech.* 146 (11), 04020123.
626 [https://doi.org/10.1061/\(ASCE\)EM.1943-7889.0001857](https://doi.org/10.1061/(ASCE)EM.1943-7889.0001857).

627 Cordier, F., Tassi, P., Claude, N., Crosato, A., Rodrigues, S., Van Bang, D.P., 2019. Numerical study of
628 alternate bars in alluvial channels with nonuniform sediment. *Water Resour. Res.* 55 (4), 2976-3003.
629 <https://doi.org/10.1029/2017WR022420>.

630 Ettema, R., 2002. Review of alluvial-channel responses to river ice. *J. Cold Reg. Eng.* 16 (4), 191-217.
631 [https://doi.org/10.1061/\(ASCE\)0887-381X\(2002\)16:4\(191\)](https://doi.org/10.1061/(ASCE)0887-381X(2002)16:4(191)).

632 Ettema, R., Braileanu, F., Muste, M., 2000. Method for estimating sediment transport in ice-covered
633 channels. *J. Cold Reg. Eng.* 14 (3), 130-144.
634 [https://doi.org/10.1061/\(ASCE\)0887-381X\(2000\)14:3\(130\)](https://doi.org/10.1061/(ASCE)0887-381X(2000)14:3(130)).

635 Gebre, S., Boissy, T., Alfredsen, K., 2014. Sensitivity to climate change of the thermal structure and ice
636 cover regime of three hydropower reservoirs. *J. Hydrol.* 510, 208-227.
637 <https://doi.org/10.1016/j.jhydrol.2013.12.023>.

638 Guo, J.K., Shan, H.Y., Xu, H.J., Bai, Y.C., Zhang, J.M., 2017. Exact solution for asymmetric turbulent
639 channel flow with applications in ice-covered rivers. *J. Hydraul. Eng.* 143 (10), 04017041.
640 [https://doi.org/10.1061/\(ASCE\)HY.1943-7900.0001360](https://doi.org/10.1061/(ASCE)HY.1943-7900.0001360).

641 Hoque, M.A., 2009. Hydraulic analysis of ice-covered river flow. M.S. thesis, Concordia University,
642 Montreal, Quebec, Canada.

643 Huang, F.B., 2014. A Numerical Model Study on River Ice and Sediment Dynamics. Ph.D. thesis,
644 Clarkson University, Potsdam, New York, United States.

645 Jha, S.K., Bombardelli, F.A., 2011. Theoretical/numerical model for the transport of non-uniform
646 suspended sediment in open channels. *Adv. Water Resour.* 34 (5), 577-591.
647 <https://doi.org/10.1016/j.advwatres.2011.02.001>.

648 Kabir, S.M.I., Ahmari, H., 2020. Evaluating the effect of sediment color on water radiance and suspended
649 sediment concentration using digital imagery. *J. Hydrol.* 589, 125189.
650 <https://doi.org/10.1016/j.jhydrol.2020.125189>.

651 Knack, I., 2011. Mathematical modeling of river dynamics with thermal-ice-sediment processes. Ph.D.
652 thesis, Clarkson University, Potsdam, New York, United States.

653 Knack, I., Shen, H.T., 2015. Sediment transport in ice-covered channels. *Int. J. Sediment Res.* 30 (1),
654 63-67. [https://doi.org/10.1016/S1001-6279\(15\)60006-3](https://doi.org/10.1016/S1001-6279(15)60006-3).

655 Krishnappan, B.G., 1983. Suspended sediment profile for ice-covered flows. *J. Hydraul. Eng.* 109 (3),
656 385-399. [https://doi.org/10.1061/\(ASCE\)0733-9429\(1983\)109:3\(385\)](https://doi.org/10.1061/(ASCE)0733-9429(1983)109:3(385)).

657 Lane, S.N., Richards, K.S., Chandler, J.H., 1996. Discharge and sediment supply controls on erosion and
658 deposition in a dynamic alluvial channel. *Geomorphology* 15 (1), 1-15.
659 [https://doi.org/10.1016/0169-555X\(95\)00113-J](https://doi.org/10.1016/0169-555X(95)00113-J).

660 Lau, Y.L., Krishnappan, B.G., 1985. Sediment transport under ice cover. *J. Hydraul. Eng.* 111 (6), 934-950.
661 [https://doi.org/10.1061/\(ASCE\)0733-9429\(1985\)111:6\(934\)](https://doi.org/10.1061/(ASCE)0733-9429(1985)111:6(934)).

662 Lawler, D.M., 1993. Needle ice processes and sediment mobilization on river banks - the River Ilston,
663 West-Glamorgan, UK. *J. Hydrol.* 150 (1), 81-114. [https://doi.org/10.1016/0022-1694\(93\)90157-5](https://doi.org/10.1016/0022-1694(93)90157-5).

664 Lorentz, H.A., 1903. Ein allgemeiner satz, die bewegung einer reibenden flüssigkeit betreffend, nebst
665 einigen anwendungen desselben. *Abh. Theor. Phys.* 1, 23.

666 Lotsari, E., Tarsa, T., Kamari, M., Alho, P., Kasvi, E., 2019. Spatial variation of flow characteristics in a
667 subarctic meandering river in ice-covered and open-channel conditions: A 2D hydrodynamic
668 modelling approach. *Earth Surf. Proc. Land.* 44 (8), 1509-1529. <https://doi.org/10.1002/esp.4589>.

669 Miyata, S., Mizugaki, S., Naito, S., Fujita, M., 2020. Application of time domain reflectometry to high
670 suspended sediment concentration measurements: Laboratory validation and preliminary field
671 observations in a steep mountain stream. *J. Hydrol.* 585, 124747.
672 <https://doi.org/10.1016/j.jhydrol.2020.124747>.

673 Muste, M., Braileanu, F., Ettema, R., 2000. Flow and sediment transport measurements in a simulated
674 ice-covered channel. *Water Resour. Res.* 36 (9), 2711-2720. <https://doi.org/10.1029/2000WR900168>.

675 Pal, D., Ghoshal, K., 2017. Hydrodynamic interaction in suspended sediment distribution of open channel
676 turbulent flow. *Appl. Math. Model.* 49, 630-646. <https://doi.org/10.1016/j.apm.2017.02.045>.

677 Peng, S.T., Dai, M.X., Zhang, J., Zhang, M.H., Shi, Q., Liang, B.C., Zheng, T.L., 2020. Dynamics of
678 ecological risks associated with heavy metals in sediments during the construction process of the

679 Yangtze River deepwater channel. J. Clean Prod. 269, 122231.
680 <https://doi.org/10.1016/j.jclepro.2020.122231>.

681 Rouse, H., 1937. Modern conceptions of the mechanics of fluid turbulence. Trans. ASCE. 102, 463-505.

682 Sayre, W.W., Song, G.B., 1979. Effects of ice covers on alluvial channel flow and sediment transport
683 processes. IIHR Report No. 218, Iowa Institute of Hydraulic Research, The University of Iowa, Iowa
684 City, Iowa.

685 Sharma, A., Herrera-Granados, O., Kumar, B., 2019. Bedload transport and temporal variation of
686 non-uniform sediment in a seepage-affected alluvial channel. Hydrol. Sci. J.-J. Sci. Hydrol. 64 (8),
687 1001-1012. <https://doi.org/10.1080/02626667.2019.1615621>.

688 Smith, B.T., Ettema, R., 1997. Flow resistance in ice-covered alluvial channels. J. Hydraul. Eng. 123 (7),
689 592-599. [https://doi.org/10.1061/\(ASCE\)0733-9429\(1997\)123:7\(592\)](https://doi.org/10.1061/(ASCE)0733-9429(1997)123:7(592)).

690 Stone, M., Krishnappan, B.G., 2002. The effect of irrigation on tile sediment transport in a headwater
691 stream. Water Res. 36 (14), 3439-3448. [https://doi.org/10.1016/S0043-1354\(02\)00073-8](https://doi.org/10.1016/S0043-1354(02)00073-8).

692 Tayfur, G., Singh, V.P., 2012. Transport capacity models for unsteady and non-equilibrium sediment
693 transport in alluvial channels. Comput. Electron. Agric. 86, 26-33.
694 <https://doi.org/10.1016/j.compag.2011.12.005>.

695 Teal, M.J., Ettema, R., Walker, J.F., 1994. Estimation of mean flow velocity in ice-covered channels. J.
696 Hydraul. Eng. 120 (12), 1385-1400. [https://doi.org/10.1061/\(ASCE\)0733-9429\(1994\)120:12\(1385\)](https://doi.org/10.1061/(ASCE)0733-9429(1994)120:12(1385)).

697 Torres, R.J., Abessa, D.M.S., Santos, F.C., Maranhão, L.A., Davanzo, M.B., do Nascimento, M.R.L.,
698 Mozeto, A.A., 2009. Effects of dredging operations on sediment quality: contaminant mobilization in
699 dredged sediments from the Port of Santos, SP, Brazil. J. Soils Sediments 9 (5), 420-432.
700 <https://doi.org/10.1007/s11368-009-0121-x>.

701 Tsai, W.F., Ettema, R., 1994. Modified eddy viscosity model in fully-developed asymmetric channel flows.
702 J. Eng. Mech. 120 (4), 720-732. [https://doi.org/10.1061/\(ASCE\)0733-9399\(1994\)120:4\(720\)](https://doi.org/10.1061/(ASCE)0733-9399(1994)120:4(720)).

703 Turcotte, B., Morse, B., Bergeron, N.E., Roy, A.G., 2011. Sediment transport in ice-affected rivers. J.
704 Hydrol. 409 (1-2), 561-577. <https://doi.org/10.1016/j.jhydrol.2011.08.009>.

705 Umeyama, M., 1992. Vertical-distribution of suspended sediment in uniform open-channel flow. J.
706 Hydraul. Eng. 118 (6), 936-941. [https://doi.org/10.1061/\(ASCE\)0733-9429\(1992\)118:6\(936\)](https://doi.org/10.1061/(ASCE)0733-9429(1992)118:6(936)).

707 van Rijn, L.C., 1984a. Sediment transport, part I: Bed load transport. J. Hydraul. Eng. 110 (10), 1431-1456.
708 [https://doi.org/10.1061/\(ASCE\)0733-9429\(1984\)110:10\(1431\)](https://doi.org/10.1061/(ASCE)0733-9429(1984)110:10(1431)).

709 van Rijn, L.C., 1984b. Sediment transport, part II: Suspended load transport. J. Hydraul. Eng. 110 (11),
710 1613-1641. [https://doi.org/10.1061/\(ASCE\)0733-9429\(1984\)110:11\(1613\)](https://doi.org/10.1061/(ASCE)0733-9429(1984)110:11(1613)).

711 Wang, F.F., Huai, W.X., Liu, M.Y, Fu, X.C., 2020. Modeling depth-averaged streamwise velocity in
712 straight trapezoidal compound channels with ice cover. J. Hydrol. 585, 124336.
713 <https://doi.org/10.1016/j.jhydrol.2019.124336>.

714 Xia, X.H., Dong, J.W., Wang, M.H., Xie, H., Xia, N., Li, H.S., Zhang, X.T., Mou, X.L., Wen, J.J., Bao,
715 Y.M., 2016. Effect of water-sediment regulation of the Xiaolangdi reservoir on the concentrations,
716 characteristics, and fluxes of suspended sediment and organic carbon in the Yellow River. Sci. Total
717 Environ. 571, 487-497. <https://doi.org/10.1016/j.scitotenv.2016.07.015>.

718 Yang, S.L., Zhang, J., Dai, S.B., Li, M., Xu, X.J., 2007. Effect of deposition and erosion within the main
719 river channel and large lakes on sediment delivery to the estuary of the Yangtze River. J. Geophys.
720 Res.-Earth Surf. 112 (F2), F02005. <https://doi.org/10.1029/2006JF000484>.

721 Zhang, R.J., 1998. River sediment dynamics (in Chinese), second ed. China Water & Power Press, Beijing.